ISSN 0027-1349, Moscow University Physics Bulletin, 2023, Vol. 78, No. 2, pp. 179–184. © Allerton Press, Inc., 2023.
ISSN 0027-1349, Moscow University Physics Bulletin, © 2023, Allerton Press, Inc., 2023.

OPTICS AND SPECTROSCOPY. LASER PHYSICS

Radiation and Transition Losses in Curved Waveguides for Bloch Surface Waves

D. A. Shilkin[1*], K. R. Safronov[1], A. D. Rozanov[1], V. O. Bessonov[1], and A. A. Fedyanin[1]

[1] *Faculty of Physics, Lomonosov Moscow State University, Moscow, 119991 Russia*

Received October 29, 2022; revised December 5, 2022; accepted December 7, 2022

Abstract—One-dimensional photonic crystals that support the propagation of Bloch surface electromagnetic waves attract the interest of researchers as an alternative platform for integrated optics with potential applications in nanophotonics, sensing, and optical manipulation of micro- and nanoparticles. In this paper, we numerically study the properties of surface wave modes in curved waveguides on top of a one-dimensional photonic crystal. It is shown that, when the waveguide is bent, an additional channel of radiation losses appears, which is associated with light leakage from the surface wave mode into bulk modes of the photonic crystal, and the waveguide mode profile becomes asymmetric with respect to the middle of the waveguide. We also determine the conditions for minimizing transition losses, which occur at the junctions of waveguides with different curvatures, by transverse displacement of the waveguide facets relative to each other.

Keywords: photonic crystals, surface electromagnetic waves, optical waveguides, eigenmodes, integrated photonics

DOI: 10.3103/S002713492302011X

INTRODUCTION

Multilayer dielectric structures are actively used in optics and photonics as they allow one to control their optical properties by changing the thicknesses and materials used [1–3]. One-dimensional photonic crystals (PCs) are multilayer structures with an alternating refractive index that have a photonic band gap and can be used as dielectric mirrors or beam splitters [4]. The presence of the photonic band gap makes it possible to excite Bloch surface electromagnetic waves (BSWs) in such structures, the field of which is concentrated at the interface between the PC and a homogeneous dielectric medium and decreases exponentially with distance from it [5–8]. The dispersion of BSWs is sensitive to the properties of the boundary layer, due to which they are used in sensorics [9–12], and the localization of the BSW field on the surface of the structure makes them a useful tool for manipulating micro- and nanoparticles in microfluidic devices [13–16].

When an additional dielectric layer is deposited on the PC surface, the BSW excitation conditions and the BSW effective refractive index change [17, 18]. For this reason, the BSW propagation can be controlled using planar optical elements on the PC surface [19–21]. This, in turn, makes such structures a promising platform for integrated photonics [22–25]. It has been shown that thin polymeric ridges can be used as waveguides for BSWs [26]. Closed in a ring, they can act as ring resonators [27, 28], and in the presence of Bragg reflectors, a localized defect mode can be excited in such structures [29]. Depending on the geometric parameters of the waveguide, it can support either one or several modes [30]. It has been shown that multimode interference can be observed in BSW waveguides, and this effect has been used to create Mach–Zehnder interferometers [31].

Curved waveguides are an essential part of many BSW-based integrated optical devices, and their mode properties differ from those of straight waveguides [32]. As in the case of standard channel waveguides [33], the profile of propagating modes undergoes changes in bent sections—the field maximum shifts relative to the center of the waveguide width—which causes the presence of transition losses at the junctions of waveguide sections with different curvature [34]. One of the methods for minimizing such losses in the case of standard channel waveguides is the displacement of the facets of sections with different curvatures relative to each

*E-mail: shilkin@nanolab.phys.msu.ru

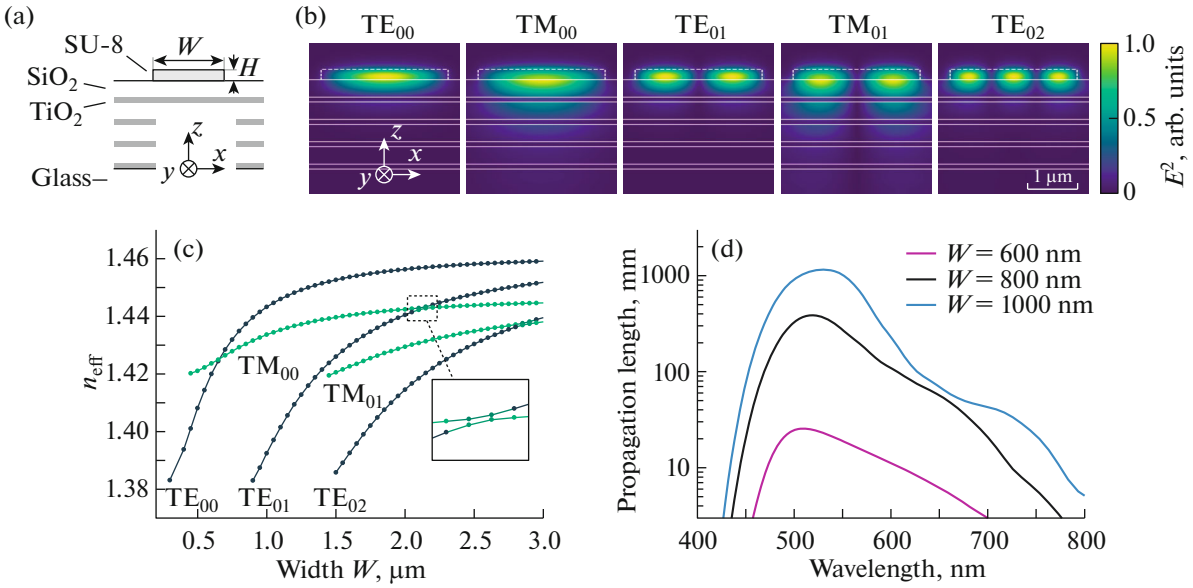

Fig. 1. (a) Schematic of the PC and the BSW waveguide. (b) Distribution of the squared electric field amplitude in the BSW modes of a waveguide with a width $W = 2.5$ μm and a height $H = 200$ nm at a wavelength of 532 nm. (c) Dependence of the effective refractive index of the supported modes at 532 nm on the waveguide width W at a fixed height $H = 200$ nm. (d) Wavelength dependence of the propagation length of the TE_{00} mode for three values of the waveguide width W at a fixed height $H = 200$ nm.

other [35]. For the case of BSWs, to the best of our knowledge, the mode matching of waveguides with different curvatures has not been previously studied.

In this paper, we numerically study the properties of BSW modes in curved waveguides on the surface of a one-dimensional PC and determine the conditions for minimizing the transition losses at the junctions of waveguides with different curvatures by transverse displacement of the waveguide facets relative to each other.

1. MODE COMPOSITION

The PC sample under study consists of 4 pairs of alternating layers of titanium oxide with a refractive index of 2.67 and silicon oxide with a refractive index of 1.46. The thicknesses of the titanium oxide and silicon oxide layers are 96.8 and 343.2 nm, respectively. The chosen thicknesses ensure low losses in the TE-polarized BSW mode at a vacuum wavelength of 532 nm [36]. The geometry of the structure is shown in Fig. 1a. The PC is located on a glass substrate with a refractive index of 1.52. The waveguide which is placed on top of the PC has a rectangular cross section of height H and width W. The waveguide material is SU-8 photopolymer with a refractive index of 1.58. Previously, this material has been successfully used to fabricate similar structures using two-photon laser lithography [30, 31]. The parameters of eigenmodes of the structure under study were determined using Lumerical FDE Solver software; the eigenvalues and eigenfunctions of the wave equation were found for an infinite waveguide with a given profile using the finite difference method. The waveguide profile was specified in a region of 10×4 μm in size, with the longer side along the x direction and the shorter side along the z direction. The distance between the waveguide and the upper boundary of the simulation region was 1.5 μm. At the boundaries of the simulation region, absorbing boundary conditions were set. A non-uniform mesh with a density of at least 14 points per material wavelength was used in the calculations. In order to verify the obtained results, calculations for selected parameters were additionally performed with an extended simulation region and a greater mesh density.

Depending on the waveguide geometry, it can support a different number of the BSW modes [30, 31]. The structure under study can support both TE- (electric field along Ox) and TM-polarized surface waves. Figure 1b shows the distribution of the squared electric field amplitude in the lowest-order modes of the waveguide with a width $W = 2.5$ μm and a height $H = 200$ nm. The mode profiles were calculated for a vacuum wavelength of 532 nm. Figure 1c shows the dependence of the effective refractive index of the supported modes at 532 nm on the waveguide width W at a fixed height $H = 200$ nm. The minimum possible value of the effective refractive index of the surface wave modes is determined by the

edge of the photonic band gap for the corresponding polarization and the chosen wavelength. For TE-polarization this value is approximately equal to 1.37, and for TM-polarization it is approximately 1.42. As the waveguide width increases, the number of the supported modes and their effective refractive indices increase. Note that in regions where TE- and TM-polarized modes have close values of the effective refractive index, the modes hybridize and anticrossing is observed if not forbidden by symmetry. This effect, which is typical for systems of coupled oscillators in the strong coupling regime [37, 38], was previously observed for the modes of standard channel waveguides [39]. For the modes of BSW waveguides this effect is discovered for the first time to our knowledge.

Figure 1d shows the wavelength dependence of the propagation length at which the field amplitude decreases by a factor of e for the TE_{00} surface wave mode. The dependence is shown for three values of the waveguide width W at a fixed height $H = 200$ nm. For example, the propagation length at 532 nm is 23 mm at a width $W = 0.6$ μm, and it is 1.16 m at $W = 1.0$ μm. Note that by changing the geometric parameters of the PC, the losses in the BSW mode can be minimized in other spectral ranges.

2. CURVED WAVEGUIDE MODE PROPERTIES

When the BSW waveguide is bent, the properties of the modes undergo significant changes. As in the case of standard channel waveguides [33, 40], the mode profile is modified and an additional channel of radiation losses appears. The geometry of calculations for the case of curved waveguides is shown in Fig. 2a; the radius of curvature R is determined by the waveguide axis shown by the dashed line. Figure 2b shows the dependence of the effective refractive index of the TE_{00} mode at a wavelength of 532 nm on the radius of curvature R for three values of the waveguide width W at a fixed height $H = 200$ nm. Note that the value of the phase front velocity is not constant inside the waveguide, but increases linearly with the distance from the center of curvature [40], which corresponds to the inversely proportional dependence of the effective refractive index on this distance. The dots in Fig. 2b show the values of the effective refractive index on the waveguide axis, and the vertical bars show the range of values within the waveguide. The minimum value corresponds to the outer boundary of the curved waveguide, and the maximum value corresponds to the inner boundary.

The BSW propagation is only possible if the propagation of bulk waves with the same tangential component of the wave vector is forbidden inside the PC. The shaded areas in Fig. 2b show the PC bands for

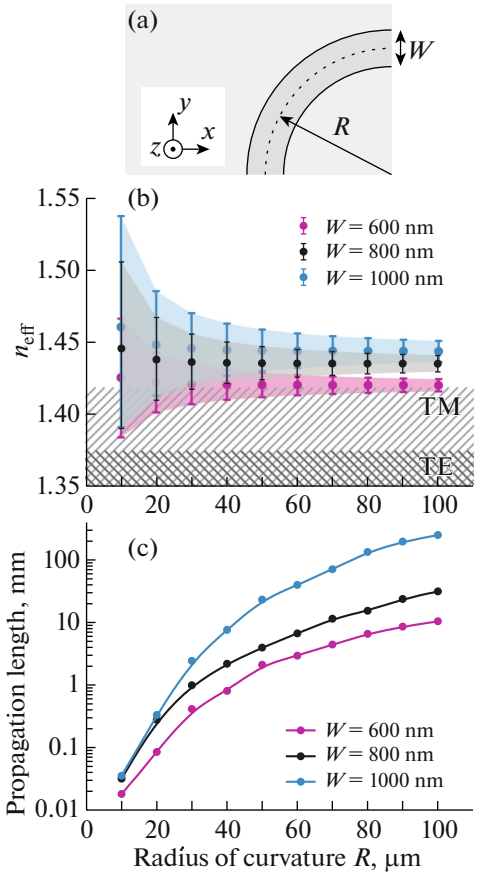

Fig. 2. (a) Calculation geometry. (b) Dependence of the effective refractive index of the TE_{00} mode on the radius of curvature R. The dots show the values on the waveguide axis; the bars show the range of values within the waveguide. The shaded areas show the PC bands for two polarizations. (c) Dependence of the propagation length of the TE_{00} mode on the waveguide radius of curvature R. The calculated data are shown by dots; the curves are guides for the eye. The waveguide height is $H = 200$ nm; calculations were carried out for a wavelength of 532 nm.

two light polarizations. For $R \geq 10$ μm and all three waveguide widths W, the effective refractive index of the TE_{00} mode within the waveguide takes values from the range that lies entirely in the photonic band gap for TE-polarization, but only partially in the band gap for TM-polarization. Due to the limited width of the waveguide, the evanescent field of the TE_{00} mode has a TM component [36], and, as a result, a part of the TM-polarized radiation can pass through the PC and leak into the substrate. Moreover, since the mode profile is not limited by the width of the waveguide, a part of radiation can also leak through TE-polarized bulk modes, and with a decrease in the radius of curvature, the fraction of such radiation increases. Thus, in addition to leakage into free space—the previously described loss mechanism in curved BSW waveguides [32]—an important role in the formation of losses in such systems is played by coupling

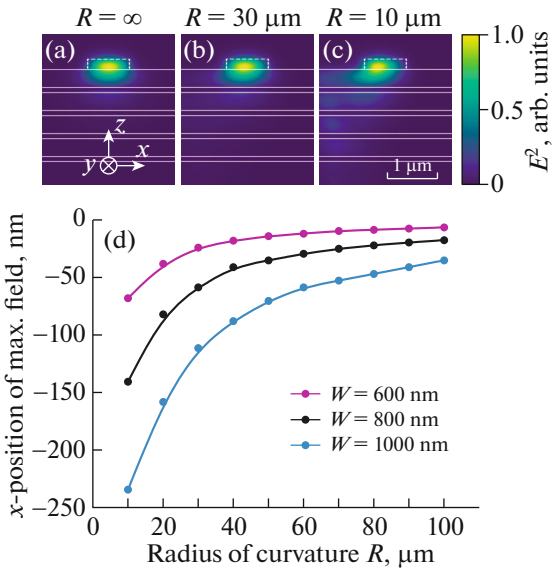

Fig. 3. (a–c) Distribution of the squared electric field amplitude in the TE_{00} surface wave mode (a) for a straight waveguide, (b) for a waveguide with a radius of curvature $R = 30$ μm, and (c) for a waveguide with a radius of curvature $R = 10$ μm. The calculation geometry is shown in Fig. 2a; the waveguide height is $H = 200$ nm, the width is $W = 800$ nm. (d) Dependence of the position of the electric field amplitude maximum in the TE_{00} mode on the waveguide radius of curvature. The calculated data are shown by dots; the curves are guides for the eye. The waveguide height is $H = 200$ nm; the position $x = 0$ corresponds to the middle of the waveguide. The calculations were carried out for a wavelength of 532 nm.

with bulk TE- and TM-polarized PC modes. The dependence of the propagation length of the TE_{00} BSW mode on the radius of curvature is shown in Fig. 2c. As the radius of curvature decreases, the losses increase significantly, and while in a straight waveguide with a width $W = 800$ nm the propagation length is approximately 0.4 m, at $R = 30$ μm it is reduced to 1 mm.

Figures 3a–3c show the distribution of the squared electric field amplitude in the TE_{00} surface wave mode for three values of the radius of curvature R. As the radius of curvature decreases, the maximum amplitude of the electric field shifts relative to the middle of the waveguide width in the direction away from the center of curvature. At $R = 10$ μm (Fig. 3c), the part of radiation for which the effective refractive index falls into the PC band leaks into the PC bulk mode. Figure 3d shows the dependence of the position of the amplitude maximum on the waveguide radius of curvature R for three values of the waveguide width W at a fixed height $H = 200$ nm. For example, in the case of a curved waveguide with a width $W = 800$ nm and a radius of curvature $R = 30$ μm, the maximum amplitude of the electric field is shifted by 60 nm.

3. MINIMIZING TRANSITION LOSSES

The data obtained highlight the importance of BSW mode matching in waveguides with different curvatures. Since the position of the amplitude maximum with respect to the waveguide axis depends on the curvature, one of the methods for minimizing transition losses at the junctions of waveguides with different curvatures is the displacement of the waveguide facets relative to each other. Figure 4 shows the dependence of the transition loss at the junction of straight and curved waveguides on the relative transverse displacement of the facets Δx. To obtain this dependence, for each displacement value a three-dimensional simulation of light propagation through the system was carried out by the finite-difference time-domain method using *Lumerical FDTD Solutions* software. The size of the simulation region was $4.0 \times 2.3 \times 4.0$ μm^3 along the x, y, and z directions, respectively. A non-uniform mesh with a density of at least 18 points per material wavelength was used in the simulations. The source was the TE_{00} mode in the straight waveguide, which was partially coupled into the mode of the curved waveguide. Upon completion of the simulation, the spatial distribution of the field and the Poynting vector flux were found at a wavelength of 532 nm in the cross section of the curved waveguide at a distance of 100 nm after the junction. Then, by calculating the overlap integral of the field distribution in this cross section and the TE_{00} eigenmode field of the curved waveguide, the fraction of the Poynting vector flux coupled into the curved waveguide mode was determined. This allowed us to estimate the transition losses with a minimum contribution from radiation losses, which are inevitably present in curved waveguides. The resulting transmission into the curved waveguide eigenmode T is maximum at a positive shift Δx. For example, for the junction of a straight waveguide and a curved one with a radius of curvature $R = 30$ μm, the transition losses are minimal when the facets are shifted by $\Delta x = 40$ nm; with respect to the case of zero shift, they are reduced by a quarter. Note that the optimal lateral shift of the facets is less than the displacement of the field amplitude maximum with respect to the waveguide axis, which is explained by the significant asymmetry of the bent waveguide mode profile.

To estimate the practical potential of the proposed method, let us compare the reduction in transition losses at a junction with radiation losses in a curved waveguide. For example, at the junction of a straight waveguide and a curved one with a radius of curvature $R = 30$ μm, 5.4% of the power is lost at zero shift and 3.9% is lost at the optimal value of Δx, i.e., the difference is 1.5%. At the same time, 1.5% of the power is lost in the same curved waveguide when propagating

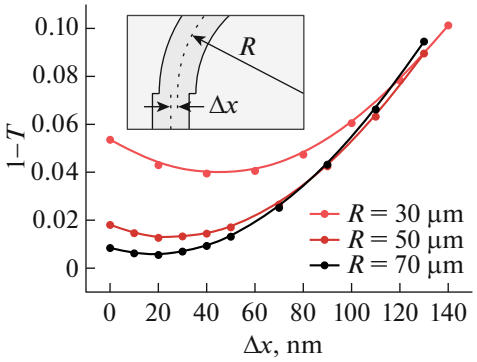

Fig. 4. Dependence of the transition losses at the junction of a straight and curved waveguides on the lateral shift Δx for three values of the radius of curvature R. The calculated data are shown by dots; the curves are guides for the eye. The waveguide height is $H = 200$ nm, the width is $W = 800$ nm. The calculations were carried out for a wavelength of 532 nm.

15 μm. Similar calculations for the junction of a straight waveguide and a curved waveguide with a radius of curvature $R = 70$ μm show that the optimal shift of the waveguide facet reduces losses by a value equivalent to the light propagation by 0.3 mm in the curved waveguide. The results obtained demonstrate the importance of optimizing the junctions of waveguides with different curvatures to minimize losses at the development of BSW-based integrated optical devices.

CONCLUSIONS

We have numerically characterized the modes of curved BSW waveguides on the surface of a one-dimensional PC. It has been shown that as the radius of curvature decreases, the radiation losses associated with the leakage of light into bulk PC modes increase, and the BSW mode profile becomes asymmetric with respect to the waveguide axis. We proposed a method for minimizing transition losses at the junctions of BSW waveguides with different curvatures by transverse displacement of the waveguide facets relative to each other. In the system under study, the proposed method allows one to reduce these losses by a quarter.

FUNDING

The study was funded by the Russian Science Foundation (project no. 21-72-00123). The authors acknowledge support from the MSU Scientific and Educational School “Photonic and Quantum technologies. Digital medicine.”

CONFLICT OF INTEREST

The authors declare that they have no conflicts of interest.

REFERENCES

1. O. S. Heavens, Rep. Prog. Phys. **23**, 1 (1960). https://doi.org/10.1088/0034-4885/23/1/301
2. R. C. Nesnidal and T. G. Walker, Appl. Opt. **35**, 2226 (1996). https://doi.org/10.1364/AO.35.002226
3. K. R. Safronov, V. O. Bessonov, and A. A. Fedyanin, JETP Letters **114**, 321 (2021). https://doi.org/10.1134/S0021364021180119
4. A. Yariv and P. Yeh, *Optical waves in crystals* (Wiley, New York, 1984).
5. W. M. Robertson, J. Light. Technol. **17**, 2013 (1999). https://doi.org/10.1109/50.802988
6. E. Descrovi, T. Sfez, L. Dominici, et al., Opt. Express **16**, 5453 (2008). https://doi.org/10.1364/OE.16.005453
7. V. V. Moskalenko, I. V. Soboleva, and A. A. Fedyanin, JETP Letters **91**, 382 (2010). https://doi.org/10.1134/S0021364010080047
8. D. A. Shilkin, E. V. Lyubin, I. V. Soboleva, and A. A. Fedyanin, J. Opt. Soc. Am. B **33**, 1120 (2016). https://doi.org/10.1364/JOSAB.33.001120
9. V. N. Konopsky and E. V. Alieva, Anal. Chem. **79**, 4729 (2007). https://doi.org/10.1021/ac070275y
10. F. Giorgis, E. Descrovi, C. Summonte, et al., Opt. Express **18**, 8087 (2010). https://doi.org/10.1364/OE.18.008087
11. A. Sinibaldi, N. Danz, E. Descrovi, et al., Sens. Actuators B Chem. **174**, 292 (2012). https://doi.org/10.1016/j.snb.2012.07.015
12. Y. Li, T. Yang, S. Song, et al., Appl. Phys. Lett. **103**, 041116 (2013). https://doi.org/10.1063/1.4816810
13. D. A. Shilkin, E. V. Lyubin, I. V. Soboleva, and A. A. Fedyanin, Opt. Lett. **40**, 4883 (2015). https://doi.org/10.1364/OL.40.004883
14. Y. Xiang, X. Tang, Y. Fu, et al., Nanoscale **12**, 1688 (2020). https://doi.org/10.1039/C9NR08399E
15. D. A. Shilkin, E. V. Lyubin, and A. A. Fedyanin, ACS Photonics **9**, 211 (2022). https://doi.org/10.1021/acsphotonics.1c01402
16. D. A. Shilkin and A. A. Fedyanin, JETP Letters **115**, 136 (2022). https://doi.org/10.1134/S0021364022030092
17. F. Villa, L. E. Regalado, F. Ramos-Mendieta, et al., Opt. Lett. **27**, 646 (2002). https://doi.org/10.1364/OL.27.000646
18. R. Dubey, E. Barakat, M. Häyrinen, et al., J. Eur. Opt. Soc. Rapid Publ. **13**, 5 (2017). https://doi.org/10.1186/s41476-016-0029-1
19. L. Yu, E. Barakat, T. Sfez, et al., Light Sci. Appl. **3**, e124 (2014). https://doi.org/10.1038/lsa.2014.5
20. E. A. Bezus, L. L. Doskolovich, D. A. Bykov, and V. A. Soifer, JETP Lett. **99**, 63 (2014). https://doi.org/10.1134/S0021364014020040

21. M. S. Kim, B. Vosoughi Lahijani, N. Descharmes, et al., ACS Photonics **4**, 1477 (2017). https://doi.org/10.1021/acsphotonics.7b00245
22. T. Kovalevich, D. Belharet, L. Robert, et al., Appl. Opt. **58**, 1757 (2019). https://doi.org/10.1364/AO.58.001757
23. D. N. Gulkin, A. A. Popkova, B. I. Afinogenov, et al., Nanophotonics **10**, 2939 (2021). https://doi.org/10.1515/nanoph-2021-0295
24. K. R. Safronov, V. O. Bessonov, D. V. Akhremenkov, et al., Laser Photonics Rev. **16**, 2100542 (2022). https://doi.org/10.1002/lpor.202100542
25. K. R. Safronov, A. A. Popkova, D. I. Markina, et al., Laser Photonics Rev. **16**, 2100728 (2022). https://doi.org/10.1002/lpor.202100728
26. E. Descrovi, T. Sfez, M. Quaglio, et al., Nano Lett. **10**, 2087 (2010). https://doi.org/10.1021/nl100481q
27. M. Menotti and M. Liscidini, J. Opt. Soc. Am. B **32**, 431 (2015). https://doi.org/10.1364/JOSAB.32.000431
28. G. A. Rodriguez, D. Aurelio, M. Liscidini, and S. M. Weiss, Appl. Phys. Lett. **115**, 011101 (2019). https://doi.org/10.1063/1.5093435
29. T. Perani, D. Aurelio, and M. Liscidini, Opt. Lett. **44**, 5133 (2019). https://doi.org/10.1364/OL.44.005133
30. K. A. Abrashitova, D. N. Gulkin, K. R. Safronov, et al., Appl. Sci. **8**, 63 (2018). https://doi.org/10.3390/app8010063
31. K. R. Safronov, D. N. Gulkin, I. M. Antropov, et al., ACS Nano **14**, 10428 (2020). https://doi.org/10.1021/acsnano.0c04301
32. X. Wu, E. Barakat, L. Yu, et al., J. Eur. Opt. Soc.: Rapid Publ. **9**, 14049 (2014). https://doi.org/10.2971/jeos.2014.14049
33. A. W. Snyder and J. D. Love, *Optical Waveguide Theory* (Chapman and Hall, New York, 1983).
34. T. Hirono, M. Kohtoku, Y. Yoshikuni, et al., IEEE Photon. Technol. Lett. **10**, 982 (1998). https://doi.org/10.1109/68.681291
35. F. Ladouceur and P. Labeye, J. Light. Technol. **13**, 481 (1995). https://doi.org/10.1109/50.372446
36. T. Perani and M. Liscidini, Opt. Lett. **45**, 6534 (2020). https://doi.org/10.1364/OL.412625
37. L. Novotny, Am. J. Phys. **78**, 1199 (2010). https://doi.org/10.1119/1.3471177
38. A. B. Lockhart, A. Skinner, W. Newman, et al., Am. J. Phys. **86**, 526 (2018). https://doi.org/10.1119/1.5036752
39. J. I. Ziegler, M. W. Pruessner, B. S. Simpkins, et al., Nanophotonics **6**, 1141 (2017). https://doi.org/10.1515/nanoph-2016-0187
40. H. Mordehai and J. Harris, IEEE J. Quantum Electron. **11**, 75 (1975). https://doi.org/10.1109/JQE.1975.1068563